HHS Public Access

Author manuscript

AJR Am J Roentgenol. Author manuscript; available in PMC 2021 October 01.

Published in final edited form as:

AJR Am J Roentgenol. 2020 October ; 215(4): 985–996. doi:10.2214/AJR.19.22571.

The Role of Dual-Phase FDG PET/CT in the Diagnosis and Follow-Up of Brain Tumors

Can Özütemiz[1], **Elizabeth C. Neil**[2], **Manoj Tanwar**[3], **Nathan T. Rubin**[4], **Kerem Ozturk**[1], **Zuzan Cayci**[1]

[1]Department of Radiology, University of Minnesota, MMC 292, 420 Delaware St SE, Minneapolis, MN 55455.

[2]Department of Neurology, University of Minnesota, Minneapolis, MN.

[3]Department of Radiology, University of Pittsburgh, Pittsburgh, PA.

[4]Biostatistics Core, Masonic Cancer Center, University of Minnesota, Minneapolis, MN.

Abstract

OBJECTIVE.—FDG PET/CT of brain tumors is limited by background activity. Dual-phase FDG PET/CT can eliminate this limitation and allow discernment of viable tumors. Our aim was to assess the diagnostic capability of dual-phase FDG PET/CT qualitatively and quantitatively and to determine cutoff values for dual-phase FDG PET/CT in brain tumor imaging.

MATERIALS AND METHODS.—Retrospectively, 51 malignant brain tumors were evaluated with dual-phase FDG PET/CT in 32 patients. Acquisitions were performed 30 minutes (time 1) and 3 hours (time 2) after administration of 10 mCi (370 MBq) FDG and 6 hours of fasting. Two observers independently and qualitatively evaluated lesions. A weighted Cohen kappa was used to calculate interrater reliability and accuracy. Quantitatively, maximum standardized uptake value (SUV_{max}) was measured in the lesions, contralateral white matter (CWM), contralateral caudate nucleus head, and ipsilateral cerebellar cortex (CC). Lesion-to-CWM SUV_{max}, lesion–to–contralateral caudate nucleus head SUV_{max}, and lesion–to–ipsilateral CC SUV_{max} ratios at time 1 and time 2 were calculated. ROC analysis was used to determine optimum cutoff values, and AUC ratios were compared among quantitative parameters. Lesion outcome was determined by pathologic results (available in 15 lesions), lesion stability on serial MRI examinations (representing nonviable tumor), or decreased tumor size on serial MRI examinations after new treatment (representing viable tumor).

RESULTS.—Thirty-seven viable and 14 nonviable lesions were evaluated. Qualitatively, the diagnostic accuracy (first observer: $\kappa = 0.45$ to $\kappa = 0.59$; second observer: $\kappa = 0.41$ to $\kappa = 0.66$) and interrater reliability (at time 1: $\kappa = 0.51$; at time 2: $\kappa = 0.83$) improved with delayed imaging. AUC and ROC analysis showed comparably high sensitivity, specificity, and accuracy profiles for early and delayed dual-phase FDG PET/CT. Some of the proposed cutoff values were as follows: lesion SUV_{max} at time 1, 7.20 (sensitivity, 89.2%; specificity, 85.7%); lesion SUV_{max} at time 2, 7.80 (sensitivity, 97.3%; specificity, 71.4%); lesion-to-CWM SUV_{max} at time 1, 2.05 (sensitivity,

Address correspondence to Z. Cayci (cayci001@umn.edu).

78.4%; specificity, 92.9%); and lesion-to-CWM SUV_{max} at time 2, 2.36 (sensitivity, 81.1%; specificity, 85.7%).

CONCLUSION.—Dual-phase FDG PET/CT improves lesion detection and diagnostic accuracy in malignant brain tumors.

Keywords

brain; delayed imaging; dual phase; FDG PET/CT; tumor

Contrast-enhanced MRI, including perfusion MRI, is the preferred imaging modality in the diagnosis and follow-up of primary and metastatic brain tumors. Standard treatment usually involves surgical resection followed by a combination of radiotherapy and chemotherapy. However, MRI may occasionally provide conflicting results for differentiation of recurrent tumor from treatment-related inflammation or pseudoresponse, greatly impacting the certainty of planned courses of therapy. This type of situation is particularly evident in the follow-up of tumors treated with radiotherapy, alkylating agents such as temozolomide, or immunotherapeutics such as bevacizumab. In addition, MRI can be contraindicated because of irremovable metal, cardiac pacemakers, or intraocular foreign bodies. These limitations can compromise a mainstay in imaging surveillance that is necessary to gauge disease response.

PET/CT can be a helpful ancillary tool, particularly for cases in which MRI delivers indeterminate results [1-3]. Although many new amino acid radiotracers, such as ^{11}Cmethylmethionine and ^{18}F-fluoroethyl-L-tyrosine, have been found to be superior to FDG in neurooncologic imaging [4-6], they are not available in many institutions in the United States because they lack Food and Drug Administration approval or the institutions lack an on-site cyclotron. Therefore, FDG is still used in many institutions because of its wide availability and reasonable price. However, the high degree of background parenchymal glucose metabolism is a well-known challenge of FDG PET/CT for intracranial lesions.

Certain methods can be used to improve the diagnostic quality and accuracy of FDG PET/CT of the brain. It has been shown that normal brain parenchymal FDG activity slightly decreases, whereas FDG activity in intracranial tumors remains relatively stable or increases over time. This has led to the development of dual-phase FDG PET/CT imaging in primary and metastatic brain tumors with improved diagnostic accuracy compared with traditional single-phase imaging [7-11]. Additionally, fusion of PET images with concurrent MRI can improve lesion detection [12, 13].

In May 2017, to evaluate possible viable tumor tissue, we began obtaining dual-phase FDG PET/CT images of treated brain tumors to fuse them with MR images when MRI results were indeterminate or as an alternative when MRI was contraindicated. This method is not standardized, so our goal was to retrospectively evaluate dual-phase FDG PET/CT findings qualitatively and quantitatively and to compare them with subsequent clinical outcomes. Our second objective was to determine specific cutoff values for dual-phase FDG PET/CT to differentiate viable tumor from nonviable lesions.

Materials and Methods

Patients

This retrospective study was approved by our institutional review board. Data for patients with primary or metastatic brain tumors that were evaluated with dual-phase FDG PET/CT at the University of Minnesota from May 2017 to February 2019 were collected from the institutional PACS using search software (Vitrea Intelligence, Vital Images). This method identified 36 examinations in 32 patients (one patient underwent three and two patients underwent two dual-phase FDG PET/CT scans at different time points; 33 scans were obtained for follow-up, three for initial diagnosis). A total of 54 target lesions were identified as evaluable. Lesions smaller than 6 mm were excluded because they were below the resolution of PET. Of the 54 target lesions, three were excluded because of a lack of prospective clinical data to validate observer response (one was secondary to bevacizumab and associated potential pseudoresponse, and two lacked prospective clinical and imaging data). Therefore, 51 lesions were included in the study.

Image Acquisition

Dual-phase FDG PET/CT protocol——All brain dual-phase FDG PET/CT studies were performed 30 minutes (time 1) and 3 hours (time 2) after IV administration of 10 mCi (370 MBq) FDG after at least 6 hours of fasting, with a blood glucose level below 180 mg/dL. All patients underwent imaging with the same PET/CT scanner (Biograph mCT64, Siemens Healthineers). The scanner was cross-calibrated between the dose calibrator and the scanner, and all clocks were synchronized. According to the protocol, imaging started with attenuation correction of CT images of the entire brain using 120 kVp, 340 mAs, and a kernel of H19s. Brain CT images were obtained and reconstructed with a slice thickness of 3 mm using a kernel of H31s with cerebrum window settings. A 10-minute emission PET scan was then performed with 400 × 400 resolution. The reconstruction method used was TrueX (Siemens Healthineers) with time-of-flight corrections. An ordered-subset expectation-maximization algorithm with eight iterations and 21 subsets was also used, with a gaussian filter. Attenuation of PET images was corrected using CT data.

MRI protocol——At the University of Minnesota, patients with brain cancer undergo contrast-enhanced MRI for radiographic surveillance at a minimum of 3-month intervals. In this study, multiple 1.5- or 3-T MRI units were used. However, a standard brain tumor protocol was used in every case that included T1-weighted imaging, fat-saturated T2-weighted imaging, FLAIR, DWI, susceptibility-weighted imaging, axial contrast-enhanced fat-saturated T1-weighted spin-echo imaging, and contrast-enhanced sagittal 3D T1-weighted magnetization-prepared rapid acquisition gradient echo (MP-RAGE) imaging with thin axial or coronal reformats. The parameters for FLAIR imaging were as follows: TR/TE, 8000–10,000/80–120; inversion time, 2400–2500 ms; slice thickness, 5 mm; matrix, 256 × 80 to 320 × 80. The parameters for T1-weighted MP-RAGE imaging were as follows: TR /TE, 1740–2400/2–4; slice thickness, 1 mm; matrix, 256 × 100. Perfusion imaging was not routinely performed, particularly for metastatic brain tumor cases which were only obtained on the clinician’s request or radiologist’s preference. For perfusion, dynamic susceptibility contrast MRI (DSC-MRI) was used with an axial echo-planar imaging

sequence (TR/TE, 2300/43; slice thickness, 5 mm; matrix, 128% × 100%). A contrast bolus (0.1 mmol/kg) was injected via power injector at a rate of 4–5 mL/s depending on the size of the IV and was then followed by a flush of 50 mL of saline at a rate of 2 mL/s.

Data Collection

Image analysis——Dual-phase FDG PET/CT images of each target lesion were evaluated both qualitatively and semiquantitatively using the MM Oncology application of syngo.via software (version VB 30a, Siemens Healthineers). Early- and delayed-phase PET images were fused with contrast-enhanced images of the most recent MRI examination. A FLAIR sequence was used for fusion in one lesion because of lack of enhancement. For five lesions, MRI was contraindicated, so dual-phase FDG PET/CT images were evaluated without MRI fusion. One staff radiologist (with fellowship training in neuroradiology and nuclear medicine) and one nuclear radiology fellow (with fellowship training in neuroradiology) independently evaluated lesions visually for qualitative assessment. The observers deemed lesions with FDG uptake higher than, equal to, or close to the background cortical activity to be viable. Lesions with no significant increase in FDG uptake relative to background uptake were deemed nonviable. Equivocal lesions that were not as FDG avid as the cortex but were slightly increased compared with background were deemed indeterminate. The observers first evaluated the early-phase image (time 1) and recorded their impression of the tumor as viable, nonviable, or indeterminate. Later, they evaluated the delayed-phase image (time 2) and again recorded their impression of the tumor. Finally, a combined assessment was performed, and the observers reported whether they felt dual imaging was helpful in the interpretation. The observers were blinded to quantitative measurements.

For semiquantitative analysis, a radiology resident subjectively placed an appropriately sized circular volume of interest (VOI) at the most suspicious region of the lesion. We call this a semiquantitative analysis because the quantitative software analysis is highly dependent on the placement of the VOI. Fusing MRI and PET data avoids inadvertent placement of the VOI over an adjacent healthy cortical structure and allows the radiologist to evaluate the area of concern on MRI and more accurately place the VOI on all three planes. Therefore, a meticulous approach was undertaken using both MRI and PET data while placing the VOI, and placement was confirmed by another observer. Lesion size and location were recorded. For normal reference, VOIs were placed in the normal-appearing contralateral white matter (CWM), contralateral caudate nucleus head, and ipsilateral cerebellar cortex (CC). These regions were selected intentionally. The CWM and contralateral caudate nucleus head were used to avoid the stagnant radiotherapy effects likely present on the treated tumor side. Also, the contralateral caudate nucleus head does not show metabolic variability, which can be seen in different parts of the cerebral cortex. The ipsilateral CC was used to eliminate possible radiotherapy effects that can be seen in the contralateral cerebellar cortex in the setting of cross-cerebellar diaschisis. The maximum standardized uptake value (SUV_{max}) was determined and used for statistical analysis. Finally, the postinfusion timing of the dual phases was recorded.

Simple ratios were calculated for each lesion related to the various reference points at time 1 and time 2: lesion-to-CWM, lesion–to–contralateral caudate nucleus head, and lesion–to–

ipsilateral CC. The ratio of lesion-to-CWM ratios was calculated by dividing the ratio at time 2 by the ratio at time 1, and percent changes in SUV_{max} were also calculated for further statistical analysis. Percent change in SUV_{max} for lesions was calculated as:

$$\frac{L_{t2} - L_{t1}}{L_{t1}} \times 100, \quad (1)$$

where L_{t1} is the SUV_{max} of the lesion at time 1 and L_{t2} is the SUV_{max} of the lesion at time 2. For lesion-to-CWM SUV_{max}, percent change was calculated as follows:

$$\frac{\frac{L_{t2}}{CWM_{t2}} - \frac{L_{t1}}{CWM_{t1}}}{\frac{L_{t1}}{CWM_{t1}}} \times 100, \quad (2)$$

where L_{t1} and CWM_{t1} are the SUV_{max} of the lesion and of the CWM at time 1, respectively, and L_{t2} and CWM_{t2} are the SUV_{max} of the lesion and of the CWM at time 2, respectively. For lesion-to-contralateral caudate nucleus head SUV_{max}, percent change was calculated as follows:

$$\frac{\frac{L_{t2}}{CCH_{t2}} - \frac{L_{t1}}{CCH_{t1}}}{\frac{L_{t1}}{CCH_{t1}}} \times 100, \quad (3)$$

where L_{t1} and CCH_{t1} are the SUV_{max} of the lesion and of the contralateral caudate nucleus head at time 1, respectively, and L_{t2} and CCH_{t2} are the SUV_{max} of the lesion and of the contralateral caudate nucleus head at time 2, respectively. For lesion-to-ipsilateral CC SUV_{max}, percent change was calculated as follows:

$$\frac{\frac{L_{t2}}{ICC_{t2}} - \frac{L_{t1}}{ICC_{t1}}}{\frac{L_{t1}}{ICC_{t1}}} \times 100, \quad (4)$$

where L_{t1} and ICC_{t1} are the SUV_{max} of the lesion and of the ipsilateral CC at time 1, respectively, and L_{t2} and ICC_{t2} are the SUV_{max} of the ipsilateral CC at time 2, respectively.

For 20 lesions, DSC-MR images were available and were analyzed by a neuroradiology fellow using DynaSuite Neuro software (version 3.1.0, Me-Vis Medical Solutions). An appropriately sized circular VOI was placed over the most suspicious area of the tumor and CWM to calculate relative cerebral blood volume (rCBV) and relative peak height (rPH) [14]. Cutoff values of 2.10 and 1.38 were used for rCBV and rPH, respectively, to determine whether the tumor was viable or nonviable [14-16].

Clinical outcome——Patients' electronic medical records were assessed for clinical outcomes. General patient characteristics, including sex, age, tumor diagnosis, prior

treatment (radiation, surgery, or chemotherapy), interval between radiotherapy and dual-phase FDG PET/CT, and any current chemotherapy, were recorded. To objectively confirm the validity of the radiologic interpretation, subsequent imaging and pathologic results and each patient's progressive clinical functional status were examined. Subsequent pathologic sampling was available in 15 lesions and served as the reference standard to confirm the accuracy and predictability of the PET examination.

Of the remaining 36 lesions for which histopathology was not available, those that remained stable in the absence of any treatment change after serial MRI examinations separated by a 6-month period were considered to be nonviable. In many cases, the treatment course was retrospectively reviewed and confirmed by the treating medical oncologist. If a new treatment was followed by a decrease in tumor size on subsequent MRI, the target lesion was considered a viable tumor. The only exception was the use of bevacizumab because of a known pseudoresponse effect; therefore, one target lesion was excluded. Four target lesions for which subsequent follow-up MRI results were not available (in the setting of death or admission to hospice) were considered viable tumors because no additional clinical treatments were available to address the progressive or recurrent cancer.

Statistical Evaluation

Comparisons of viable and nonviable lesions were performed using chi-square tests for the qualitative assessments and two-sample *t* tests for the semiquantitative parameters. Comparisons of time 1 and time 2 for the semiquantitative parameters were performed using paired *t* tests separately for the viable and nonviable lesions. Interactions between lesion type (viable vs nonviable) and time were also assessed using linear regression models for the semiquantitative parameters. Because of the presence of indeterminate assessments, the accuracy of each observer's qualitative assessment at both time points was calculated using a weighted Cohen kappa. Interrater reliability at each time point was also calculated using a weighted Cohen kappa. For semiquantitative analysis, ROC curves and AUCs were calculated for various PET parameters. Optimal cutoff points were determined by minimizing the distance between 100% sensitivity or 100% specificity and the ROC curve. Various PET parameters (e.g., accuracy, sensitivity, specificity) were calculated using these optimal cutoff points. A subgroup analysis was performed among lesions with DSC-MRI data. Analyses were performed with R software (version 3.6.0, R Foundation), and *p* values less than 0.05 were considered statistically significant.

Results

Fifty-one lesions in 32 patients (23 women, nine men) with a mean age of 59 years old (range, 35–84 years) were included. Histology was as follows: 22 primary high-grade brain neoplasms (grade IV glioblastoma multiforme, 20; grade III anaplastic astrocytoma, 2), 26 metastatic lesions (breast, 12; lung, 7; ovaries, 5; melanoma, 1; endometrium, 1), and three primary CNS lymphomas. Clinical outcome analysis revealed 10 viable and five nonviable lesions in 15 lesions with available histology. Of the 36 lesions without available pathologic results, 27 were considered viable and nine were considered nonviable using our study criteria. In total, 37 lesions were deemed viable. Mean lesion size was 20 mm (range, 7–62

mm). When the viable and nonviable tumor groups were compared, no significant differences were seen in age, sex, diagnosis, lesion size, lesion location, or acquisition time ($p > 0.05$).

Qualitative Assessment

A summary of the two observers' subjective analyses of the lesions is given in Table 1 and Figures 1 and 2. As seen in Table 1, the number of indeterminate results decreased for both observers after viewing the delayed images, and diagnostic accuracy was markedly improved in the combined assessment. Diagnostic accuracy improved for both the first observer (from $\kappa = 0.45$ to $\kappa = 0.59$) and the second observer (from $\kappa = 0.41$ to $\kappa = 0.66$). The first observer thought dual imaging was helpful in evaluation of 36 of the 51 lesions (70.6%); the second observer thought it was helpful in 41 of 51 lesions (80.4%). Regarding interrater reliability, there was a weak agreement between the observers at time 1 ($\kappa = 0.51$), which increased to strong agreement at time 2 ($\kappa = 0.83$).

Semiquantitative Assessment

Viable lesions had significantly higher lesion SUV_{max}, lesion-to-CWM SUV_{max}, lesion–to–contralateral caudate nucleus head SUV_{max}, and lesion–to–ipsilateral CC SUV_{max} compared with nonviable lesions at both time points (Table 2). SUV_{max} significantly increased from time 1 to time 2 for both nonviable and viable lesions ($p = 0.010$ and $p < 0.001$, respectively). However, for lesion-to-CWM SUV_{max}, lesion–to–contralateral caudate nucleus head SUV_{max}, and lesion–to–ipsilateral CC SUV_{max}, the increase was only significant for the viable lesions (viable: $p < 0.001$ for all; nonviable: $p = 0.147$ for lesion-to-CWM, $p = 0.984$ for lesion–to–contralateral caudate nucleus head, $p = 0.227$ for lesion–to–ipsilateral CC). In addition, none of the interactions were statistically significant (lesion SUV_{max}, $p = 0.180$; lesion-to-CWM SUV_{max}, $p = 0.152$; lesion–to–contralateral caudate nucleus head SUV_{max}, $p = 0.176$; lesion–to–ipsilateral CC SUV_{max}, $p = 0.124$), suggesting that the increase from time 1 to time 2 does not significantly differ by lesion type. Figure 3 sets out the ROC curves; AUC values showed similar and comparable results for time 1 and time 2 with the highest AUC of 92.1% using lesion SUV_{max} at time 1. The percent changes of these different parameters were not as pronounced as individual lesion SUV_{max} values or ratios for any specific phase when differentiating viable from nonviable tumor (Table 2 and Fig. 3). Only lesion–to–contralateral caudate nucleus head percent change showed a statistically significant result with a markedly lower AUC value.

Table 2 summarizes the comparison of mean values for each parameter at time 1 and time 2 for both viable and nonviable lesions. All reference points showed statistically similar results between viable and nonviable lesions ($p > 0.05$), allowing appropriate reference for each anatomic location. Only ipsilateral CC at time 1 was close to the margin of statistically significant difference ($p = 0.067$).

Table 3 details the optimal cutoff values calculated from the ROC analysis for each parameter at time 1 and time 2. The AUC value, diagnostic accuracy, sensitivity, specificity, positive predictive value, and negative predictive value were calculated for each parameter.

Comparison of Dynamic Susceptibility Contrast MRI and Dual-Phase FDG PET/CT

Table 4 summarizes the comparison of field-defined cutoff values for DSC-MRI parameters (rCBV and rPH) and dual-phase FDG PET/CT parameters defined by ROC analysis. DSC-MRI parameters showed greater sensitivity with relatively low accuracy and specificity. In comparison, dual-phase FDG PET/CT parameters, in general, provided greater accuracy and specificity. In particular, lesion SUV_{max} at time 2 showed greater accuracy, sensitivity, and specificity compared with DSC-MRI data.

Selected examples of brain lesions are shown in Figures 4-6.

Discussion

In addition to MRI, PET has been used as an adjunctive modality to improve lesion interpretation in patients with brain cancer. Although both MRI and PET have limitations, the diagnostic accuracy can improve with the use of a combined imaging approach. In particular, for PET using FDG, dual-phase imaging has shown improved visual recognition of primary brain tumor with better lesion differentiation from the background brain tissue [10]. Spence et al. [10] reported a nearly 20% increase in tumor–to–white matter ratio with dual-phase imaging separated by 3 hours and in lesion–to–gray matter (GM) ratio with imaging separated by 5 hours, although the exact underlying mechanism for this finding is not known. Typically, glucose is trapped within the cells after phosphorylation with hexokinase [17]. Astrocytes have been found to contain glucose-6-phosphatase, which removes the phosphate group from glucose-6-phosphate; glucose is then exported from the cell via glucose transporter membrane proteins [18]. This mechanism may also play a role in decreased FDG retention in normal brain parenchyma over time. Glucose-6-phosphatase activity is hypothesized to be reduced in cancer cells, thus further contributing to the difference in FDG retention between normal cells and cancer cells [10].

Another method to improve lesion characterization is fusion of PET and MRI data. Whereas PET provides metabolic data, the anatomic detail seen in MR images can raise more suspicion of even smaller areas within lesions and, thus, better differentiate malignant metabolic activity with higher accuracy [12, 13].

Glucose loading before PET may also improve lesion detection. When blood glucose levels are high, FDG competes with the glucose in circulation, which decreases the likelihood of FDG uptake by normal brain parenchyma [11, 19, 20]. However, the current patient preparation protocol for FDG PET/CT brain tumor imaging includes 4–6 hours of fasting before FDG administration [1]. In addition to this suggested protocol, we apply delayed imaging. Therefore, in this study, our aim was to investigate the role of delayed acquisition without using glucose loading.

No well-defined quantitative cutoff values have been established for single-phase or dual-phase FDG PET/CT of brain tumors [1]. Consequently, an objective of this study was to determine cutoff values that can translate to clinical usage and serve as standards for future studies involving dual-phase FDG PET/CT. Prior studies of single-phase PET scans acquired at 1 hour typically have used prespecified lesion SUV_{max} or a lesion-to-CWM SUV_{max} ratio.

For example, a ratio of 1.75 was recommended for lesion-to-CWM SUV_{max} in metastatic lesions, resulting in a sensitivity of 87.5% and specificity of 32% [12]. Leiva-Salinas et al. [13] found that lesions with lesion-to-CWM SUV_{max} ratios of 2, 2.5, or higher resulted in worse outcomes compared with ratios of 1.7 in patients with primary brain tumors.

We are aware of only a few studies that have examined the utility of dual-phase FDG PET/CT in brain tumors, which have yielded different recommendations and results. In a study that included 22 metastatic and primary brain tumors and compared low-grade and high-grade lesions, data showed a significant difference in lesion SUV_{max} between time 1 and time 2, although there was no difference between groups regarding percent change [21]. Similar to our study, all patients underwent PET/CT after 6-hour fasting. According to a study by Horky et al. [8], which investigated 27 metastatic lesions in 25 patients, the most useful and accurate parameters to differentiate radiation necrosis from viable tumors were lesion-to-GM percent change, lesion-to-CWM percent change, lesion-to-GM at time 2, and lesion-to-CWM at time 2 using SUV_{max}. Their proposed cutoff values, relative sensitivity, and specificity were as follows: 19%, 94.7%, and 100%, respectively, for lesion-to-GM percent change; 25%, 89.4%, and 90.9% for lesion-to-CWM percent change; 1, 78.9%, and 100% for lesion-to-GM at time 2; and 1.72, 100%, and 81.8% for lesion-to-CWM at time 2 [8]. In our study, parameters such as lesion–to–contralateral caudate nucleus head percent change and lesion-to-CWM percent change were found to have little correlative predictability or clinical utility. These differences can be explained by variations in imaging protocols used by Horky et al. and by our group. First, Horky et al. permitted patients to eat between early and delayed imaging. Second, they used contralateral frontal cortical GM as a reference point. In our view, the contralateral caudate nucleus head and ipsilateral CC are more reliable reference points because of the concrete nature of the anatomic landmarks and the stability of the metabolic activity.

The diagnostic performance of DSC-MRI varies from study to study. Mitsuya et al. [15] found 100% sensitivity and 95% specificity using an rCBV cutoff of 2.10 to differentiate metastasis from radiation necrosis. Matsusue et al. [16] used the same value but found 85%, 90%, and 80% values for accuracy, sensitivity, and specificity, respectively. Although these studies contained a small number of lesions, the numbers were comparable with our small subgroup analysis. Regarding rPH, Barajas et al. [14] found a sensitivity of 89% and specificity of 81% using a cutoff of 1.38 in discrimination of glioblastoma multiforme from radiation necrosis while using a cutoff of 1.70 for rCBV with unreliable results. These studies indicate that DSC-MRI has a good sensitivity profile with relatively lower specificity, leading to a missed diagnosis in 10–20% of cases. In our small study population, DSC-MRI also had a high sensitivity profile, although a lower specificity and accuracy profile was found compared with dual-phase FDG PET/CT. Among different PET parameters, the best accuracy (85%), sensitivity (91.7%), and specificity (75.0%) were obtained using a cutoff value of 7.80 for lesion SUV_{max} in the 3-hour delayed imaging. However, this analysis should not be used for direct comparison of these two imaging methods because our DSC-MRI data came from a selected case series in which clinical and radiologic progression could not be clearly identified; therefore, additional dual-phase FDG PET/CT examinations were performed. However, it should provide an idea about the

benefits and efficacy of using dual-phase FDG PET/CT when conventional MRI and DSC-MRI results are indeterminate.

Our data indicate that dual-phase FDG PET/CT provides increased lesion detection and diagnostic accuracy for patients with primary and secondary brain cancer. The delayed phase significantly contributes to a decrease in indeterminate results. According to our experience, dual-phase imaging was not overly inconvenient to patients and did not pose scheduling difficulties within the department. Although the data acquired at the early time point provided good comparison imaging with a limited amount of additional radiation exposure, if patient inconvenience or scheduling concerns are thought to impede adoption of this imaging protocol at a cancer center, then single-phase imaging data acquired at 3 hours could be used with a similar diagnostic accuracy. This conclusion is supported by an increase in both interobserver reliability and strong agreement at time 2 and is echoed in the findings of Spence et al. [10] and Bochev et al. [7].

This study has several advantages. First, to our knowledge, it is the largest study investigating the utility of dual-phase FDG PET/CT in primary and metastatic brain tumors. Second, we used fusion of MRI with PET for better lesion identification and delineation. Next, perfusion DSC-MRI and dual-phase FDG PET/CT were compared; to our knowledge, our study is the first to make this comparison. Finally, new cutoff values for both early and delayed acquisition were proposed for use in routine clinical practice and future studies.

This study has certain limitations. First are the known limitations of a retrospective design. In addition, the study sample could be considered small despite being, to our knowledge, the largest of any study examining dual-phase FDG PET/CT. Finally, the clinical outcome was not fully defined by pathologic results as the reference standard, and although all available data were used, including follow-up imaging and clinical assessment, biased results cannot be clearly excluded for cases in which histopathology was not available.

Conclusion

Overall, dual-phase FDG PET/CT fused with MRI improves lesion detection and diagnostic accuracy in primary and metastatic brain cancer. With the introduction of 3-hour delayed imaging, qualitative interrater reliability is improved, and indeterminate results are decreased. Optimal cutoff values using lesion SUV_{max}, lesion-to-CWM SUV_{max}, lesion–to–contralateral caudate nucleus head SUV_{max}, and lesion–to–ipsilateral CC SUV_{max} for early and delayed acquisition showed comparable results with high diagnostic accuracy, sensitivity, and specificity. On the basis of this information, an alternative single-phase imaging protocol acquired at 3 hours might be optimal without early-phase imaging. Radiologists should use dual-phase imaging for improved qualitative assessment, and with the addition of the semiquantitative analysis using the aforementioned values, diagnostic accuracy further improves, particularly in cases where perfusion DSC-MRI shows indiscernible results.

Acknowledgments

We thank our PET/CT technicians Todd Kes and Cassandra Koldenhoven for their contribution to obtaining these PET/CT examinations over 3 years, MRI technician Jim Singh for providing technical details in MRI acquisition, and Paul W. Sperduto for obtaining additional clinical outcome data for patients referred from outside facilities.

References

1. Law I, Albert NL, Arbizu J, et al. Joint EANM/EANO/RANO practice guidelines/SNMMI procedure standards for imaging of gliomas using PET with radiolabelled amino acids and [^{18}F]FDG: version 1.0. Eur J Nucl Med Mol Imaging 2019; 46:540–557 [PubMed: 30519867]
2. Galldiks N, Langen KJ, Albert NL, et al. PET imaging in patients with brain metastasis: report of the RANO/PET group. Neuro Oncol 2019; 21:585–595 [PubMed: 30615138]
3. Meric K, Killeen RP, Abi-Ghanem AS, et al. The use of ^{18}F-FDG PET ratios in the differential diagnosis of common malignant brain tumors. Clin Imaging 2015; 39:970–974 [PubMed: 26259864]
4. Dunet V, Pomoni A, Hottinger A, Nicod-Lalonde M, Prior JO. Performance of ^{18}F-FET versus ^{18}F-FDG-PET for the diagnosis and grading of brain tumors: systematic review and meta-analysis. Neuro Oncol 2016; 18:426–434 [PubMed: 26243791]
5. Katsanos AH, Alexiou GA, Fotopoulos AD, Jabbour P, Kyritsis AP, Sioka C. Performance of ^{18}F-FDG, ^{11}C-methionine, and ^{18}F-FET PET for glioma grading: a meta-analysis. Clin Nucl Med 2019; 44:864–869 [PubMed: 31205150]
6. Tomura N, Kokubun M, Saginoya T, Mizuno Y, Kikuchi Y. Differentiation between treatment-induced necrosis and recurrent tumors in patients with metastatic brain tumors: comparison among ^{11}C-methionine-PET, FDG-PET, MR permeability imaging, and MRI-ADC—preliminary results. AJNR 2017; 38:1520–1527 [PubMed: 28619837]
7. Bochev PH, Klisarova A, Kaprelyan AG, Chaushev B, Dancheva Z. Delayed FDG-PET/CT images in patients with brain tumors: impact on visual and semiquantitative assessment. J IMAB 2013; 19:367–371
8. Horky LL, Hsiao EM, Weiss SE, Drappatz J, Gerbaudo VH. Dual phase FDG-PET imaging of brain metastases provides superior assessment of recurrence versus post-treatment necrosis. J Neurooncol 2011; 103:137–146 [PubMed: 20838854]
9. Prieto E, Martí-Climent JM, Domínguez-Prado I, et al. Voxel-based analysis of dual-time-point ^{18}F-FDG PET images for brain tumor identification and delineation. J Nucl Med 2011; 52:865–872 [PubMed: 21571807]
10. Spence AM, Muzi M, Mankoff DA, et al. ^{18}F-FDG PET of gliomas at delayed intervals: improved distinction between tumor and normal gray matter. J Nucl Med 2004; 45:1653–1659 [PubMed: 15471829]
11. Farid K, Sibon I, Fernandez P, Guyot M, Jeandot R, Allard M. Delayed acquisition and hyperglycemia improve brain metastasis detection on F-18 FDG PET. Clin Nucl Med 2009; 34:533–534 [PubMed: 19617738]
12. Leiva-Salinas C, Muttikkal TJE, Flors L, et al. FDG PET/MRI coregistration helps predict response to gamma knife radiosurgery in patients with brain metastases. AJR 2019; 212:425–430 [PubMed: 30422717]
13. Leiva-Salinas C, Schiff D, Flors L, Patrie JT, Rehm PK. FDG PET/MR imaging coregistration helps predict survival in patients with glioblastoma and radiologic progression after standard of care treatment. Radiology 2017; 283:508–514 [PubMed: 28234553]
14. Barajas RF Jr, Chang JS, Segal MR, et al. Differentiation of recurrent glioblastoma multiforme from radiation necrosis after external beam radiation therapy with dynamic susceptibility-weighted contrast-enhanced perfusion MR imaging. Radiology 2009; 253:486–496 [PubMed: 19789240]
15. Mitsuya K, Nakasu Y, Horiguchi S, et al. Perfusion weighted magnetic resonance imaging to distinguish the recurrence of metastatic brain tumors from radiation necrosis after stereotactic radiosurgery. J Neurooncol 2010; 99:81–88 [PubMed: 20058049]

16. Matsusue E, Fink JR, Rockhill JK, Ogawa T, Maravilla KR. Distinction between glioma progression and post-radiation change by combined physiologic MR imaging. Neuroradiology 2010; 52:297–306 [PubMed: 19834699]
17. Lai JC, Behar KL, Liang BB, Hertz L. Hexokinase in astrocytes: kinetic and regulatory properties. Metab Brain Dis 1999; 14:125–133 [PubMed: 10488914]
18. Ghosh A, Cheung YY, Mansfield BC, Chou JY. Brain contains a functional glucose-6-phosphatase complex capable of endogenous glucose production. J Biol Chem 2005; 280:11114–11119 [PubMed: 15661744]
19. Ishizu K, Nishizawa S, Yonekura Y, et al. Effects of hyperglycemia on FDG uptake in human brain and glioma. J Nucl Med 1994; 35:1104–1109 [PubMed: 8014665]
20. Seo YS, Chung TW, Kim IY, Bom HS, Min JJ. Enhanced detectability of recurrent brain tumor using glucose-loading F-18 FDG PET. Clin Nucl Med 2008; 33:32–33 [PubMed: 18097254]
21. Kim DW, Kim CG, Park SA, Jung SA. Experience of dual time point brain F-18 FDG PET/CT imaging in patients with infectious disease. Nucl Med Mol Imaging 2010; 44:137–142 [PubMed: 25013525]

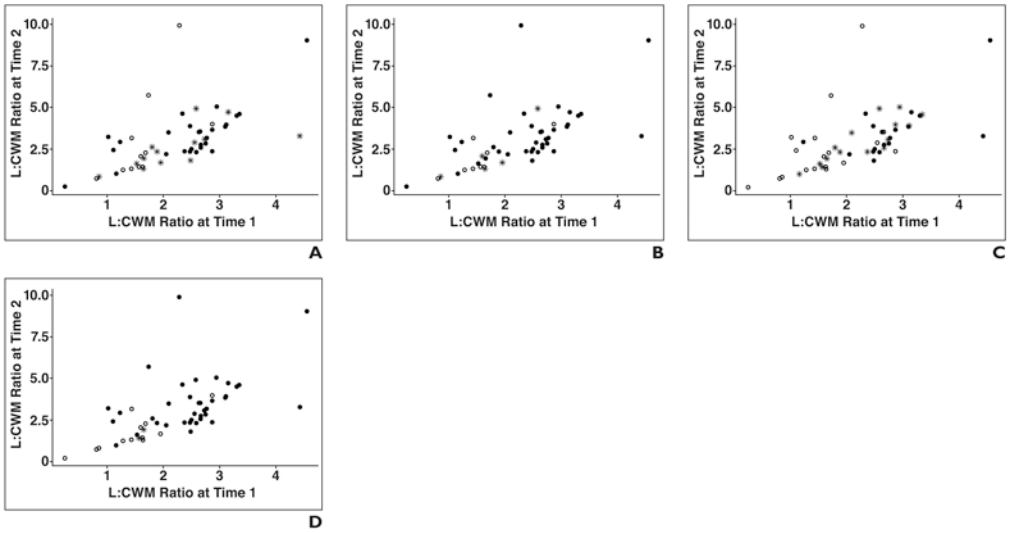

Fig. 1—.

Subjective qualitative determinations of nature of lesion combined with semiquantitative lesion–to–contralateral white matter (L:CWM) ratios. Observers reviewed same images of 51 tumors in 32 patients to allow comparison of determinations. Solid circles, open circles, and stars represent observer determinations that lesion was viable tumor, nonviable tumor, or indeterminate, respectively.

A–D, Scatterplots show qualitative assessment of lesions as nonviable, viable, or indeterminate by staff radiologist observer at time 1 (**A**) and time 2 (**B**) and by nuclear radiology fellow at time 1 (**C**) and time 2 (**D**). Both observers designated fewer lesions as indeterminate after seeing delayed images. In addition, some lesions initially deemed to be nonviable in early phase were deemed viable after viewing delayed imaging. For those lesions, lesion-to-CWM ratio was less than 2 in early phase but greater than 2 in delayed phase.

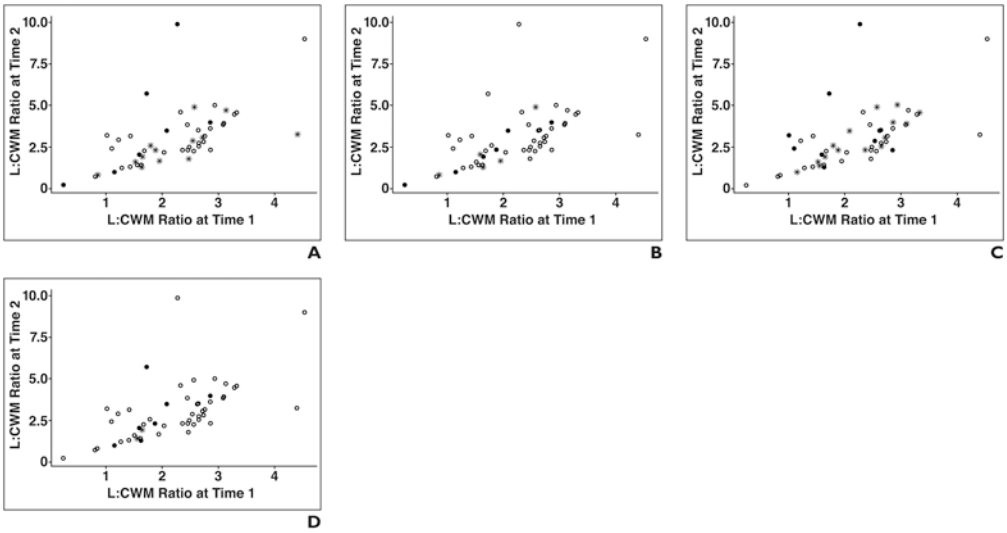

Fig. 2—.

Accuracy of subjective qualitative determinations of nature of lesion when compared with semiquantitative lesion–to–contralateral white matter (L:CWM) ratios. Observers reviewed same images of 51 tumors in 32 patients to allow comparison of determinations. Solid circles, open circles, and stars represent observer determinations that determination was inaccurate, accurate, or indeterminate, respectively.

A–D, Scatterplots show qualitative assessments by staff radiologist observer at time 1 (**A**) and time 2 (**B**) and by nuclear radiology fellow at time 1 (**C**) and time 2 (**D**). After seeing delayed images, designations of nature of lesion as indeterminate were more accurate and number of inaccurate determinations decreased for both observers.

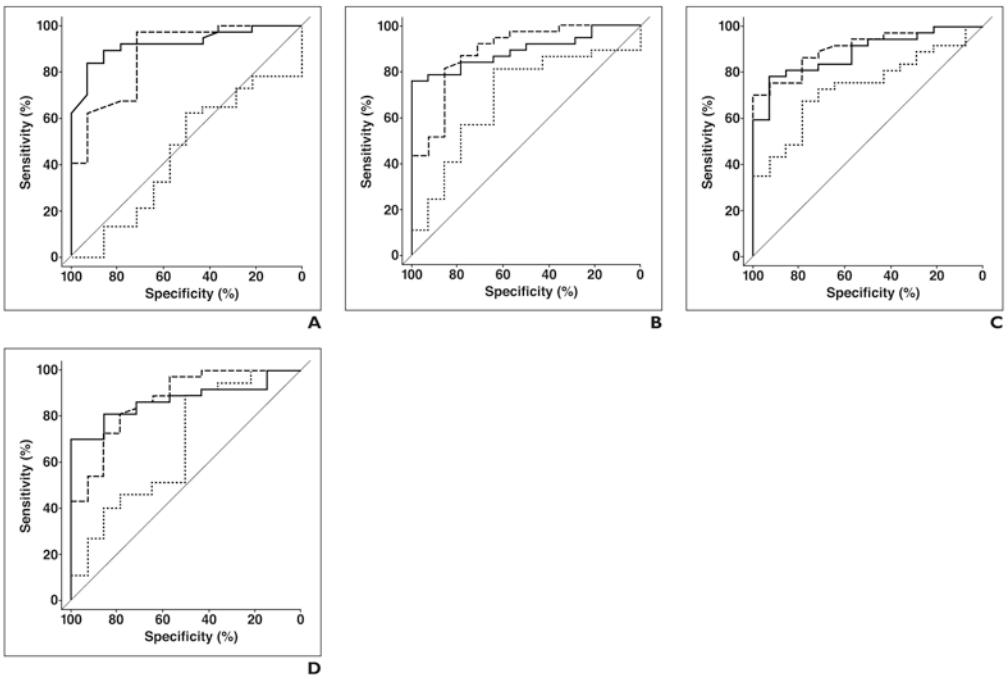

Fig. 3—.

ROC analysis for early phase (*solid black line*), delayed phase (*dashed line*), and percent change (*dotted line*). Gray diagonal line is line of reference.

A, Graph shows analysis of lesion maximum standardized uptake value (SUV_{max}). In early and delayed phases, AUCs were 92.1% and 87.5%, respectively, with percent change of 45.0%.

B, Graph shows analysis of ratio of lesion SUV_{max} to contralateral white matter SUV_{max}. In early and delayed phases, AUCs were 89.0% and 88.7%, respectively, with percent change of 68.5%.

C, Graph shows analysis of ratio of lesion SUV_{max} to contralateral caudate nucleus head SUV_{max}. In early and delayed phases, AUCs were 88.6% and 90.8%, respectively, with percent change of 73.7%.

D, Graph shows analysis of ratio of lesion SUV_{max} to ipsilateral cerebellar cortex SUV_{max}. In early and delayed phases, AUCs were 87.3% and 87.4%, respectively, with percent change of 67.4%.

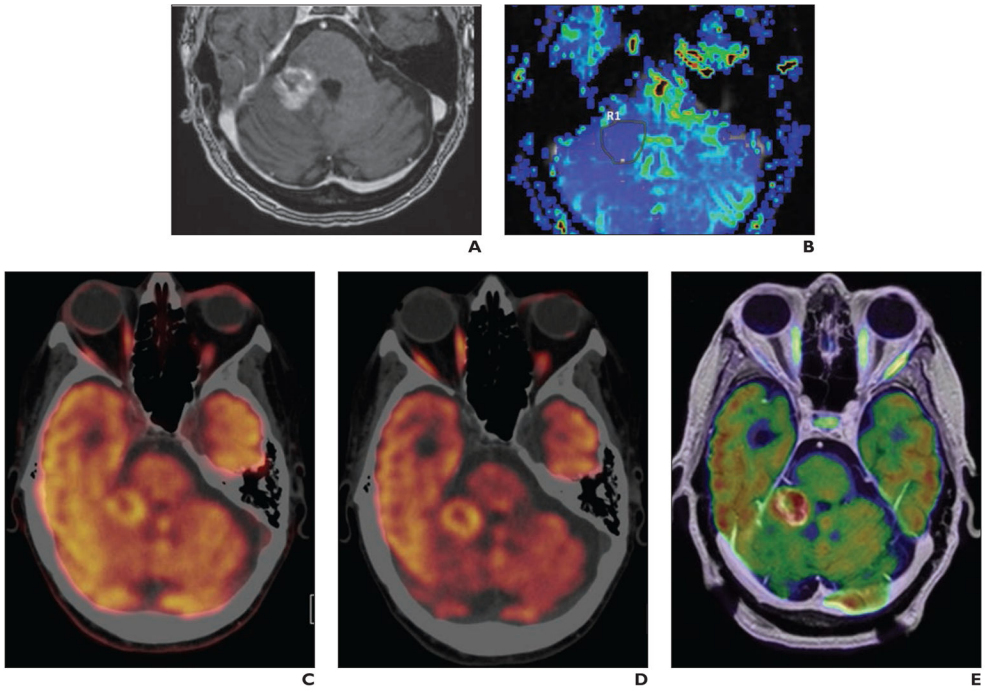

Fig. 4—.

84-year-old man with metastatic lung cancer who underwent stereotactic gamma knife treatment to right cerebellar peduncle lesion 18 months before.

A and **B,** Follow-up MR image (**A**) shows increasing enhancement at treatment site, which was deemed to be radiation necrosis after negative perfusion MR image (**B**) relative peak height of 0.3 and relative cerebral blood volume of 0.6 in treatment site ROI (R1, *outline*). **C** and **D,** On early (**C**) and delayed (**D**) PET/CT images obtained to assess progression, lesion shows ringlike peripheral FDG uptake, consistent with tumor recurrence. In general, tumoral activity is better seen on delayed imaging because of decreased background activity. **E,** Fusion of delayed PET and MRI show metabolic activity corresponding with enhancing regions. Lesion maximum standardized uptake values (SUV_{max}) were 12.4 on early images and 22.4 on delayed images (80% increase) with corresponding contralateral white matter (CWM) SUV_{max} values of 4 and 5.7, yielding ratios of lesion SUV_{max} to CWM SUV_{max} of 3.1 and 3.9, respectively. Patient again underwent gamma knife treatment; follow-up images (not shown) showed decreased enhancement.

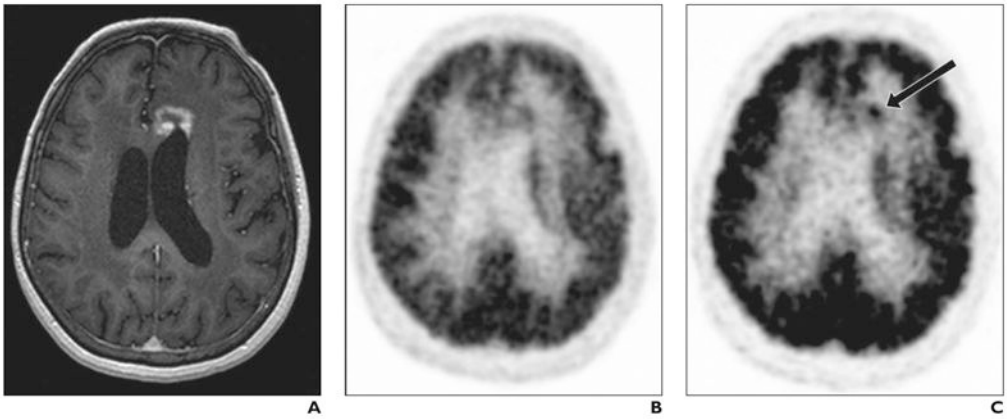

Fig. 5—.

67-year-old woman with metastatic breast cancer who had previously undergone whole-brain radiation and stereotactic radiosurgery to treat lesion in genu of corpus callosum. On 3-month follow-up images (not shown), lesion was markedly smaller.

A, Twelve-month follow-up MR image shows enlarging mass on treatment side, which could represent either radiation necrosis or recurrence.

B, Early dual-phase FDG PET image shows lesion designated as radiation necrosis by both observers on visual assessment (maximum standardized uptake value [SUV_{max}], 5).

C, Delayed FDG PET image shows marked uptake (SUV_{max}, 10.3) within tumor, particularly in anterolateral aspect of target lesion (*arrow*), which was designated as recurrent tumor by both observers. Even though relative decrease or stability in background activity is expected in most cases, background may also show significantly increased uptake in some cases. Cutoff values could be useful in these situations. In this case, lesion–to–contralateral white matter ratios in early and delayed phases were 1.4 and 2.5, respectively. Patient underwent stereotactic gamma knife treatment with lesion stability in future follow-ups (not shown).

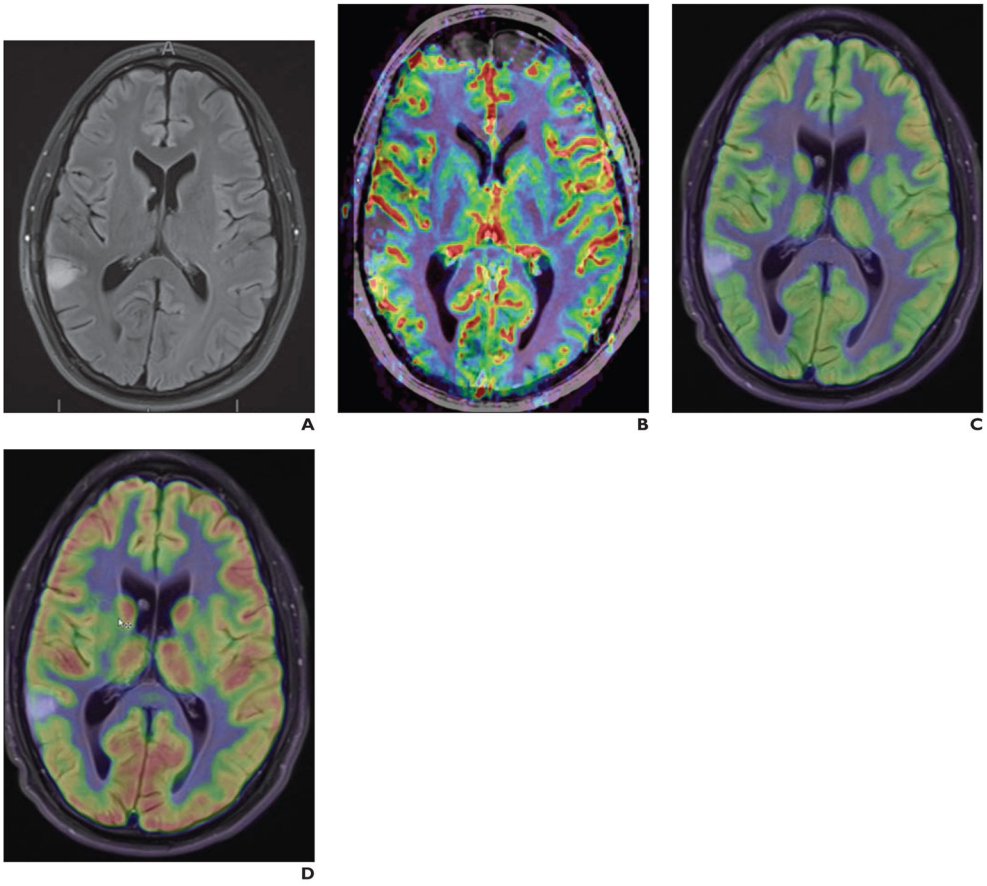

Fig. 6—.

36-year-old man who underwent surgical resection of glioblastoma multiforme and subsequent treatment with concurrent temozolomide and radiotherapy 5 months before.

A, Follow-up MR image shows T2 hyperintense nonenhancing masslike lesion in right temporal lobe that is distant from initial surgical resection cavity but is within area of previous radiotherapy.

B, Despite concern for recurrence, perfusion MR image shows negative finding with relative peak height of 0.25 and relative cerebral blood volume of 0.3. For further assessment, patient underwent FLAIR-fused PET/CT.

C and **D,** Early (**C**) and delayed (**D**) FLAIR-fused PET/CT images show lesion that both observers designated as radiation necrosis on both early and delayed images. On early images, maximum standardized uptake value (SUV_{max}) of lesion was 6.4 and that of contralateral white matter (CWM) was 3.0, yielding ratio of 2.1. On delayed images, SUV_{max} was 8.6 for lesion and 3.7 for CWM, yielding ratio of 2.3. Percent change for lesion was 34%. On follow-up imaging (not shown), this area had grown with new enhancement, so patient underwent biopsy, which revealed viable glioblastoma. Although observers did not reach correct diagnosis with visual assessment, use of determined quantitative cutoff values could have been led to this case being correctly identified as representing viable tumor.

TABLE 1:

Comparison of Visual Qualitative Assessments of Viable and Nonviable Lesions by Two Observers

Visual Assessment	Nonviable Lesion (*n* = 14)	Viable Lesion (*n* = 37)	Total (*n* = 51)	*p*
Staff radiologist				
Early phase				0.004
Viable	3 (21.4)	24 (64.9)	27 (52.9)	
Nonviable	7 (50.0)	4 (10.8)	11 (21.6)	
Indeterminate	4 (28.6)	9 (24.3)	13 (25.5)	
Delayed phase				< 0.001
Viable	5 (35.7)	33 (89.2)	38 (74.5)	
Nonviable	7 (50.0)	1 (2.7)	8 (15.7)	
Indeterminate	2 (14.3)	3 (8.1)	5 (9.8)	
Combined assessment				< 0.001
Viable	5 (35.7)	33 (89.2)	38 (74.5)	
Nonviable	7 (50.0)	2 (5.4)	9 (17.6)	
Indeterminate	2 (14.3)	2 (5.4)	4 (7.8)	
Dual imaging helpful				0.047
Yes	7 (50.0)	29 (78.4)	36 (70.6)	
No	7 (50.0)	8 (21.6)	15 (29.4)	
Nuclear radiology fellow				
Early phase				0.003
Viable	0 (0.0)	18 (48.6)	18 (35.3)	
Nonviable	9 (64.3)	9 (24.3)	18 (35.3)	
Indeterminate	5 (35.7)	10 (27.0)	15 (29.4)	
Delayed phase				< 0.001
Viable	3 (21.4)	34 (91.9)	37 (72.5)	
Nonviable	9 (64.3)	3 (8.1)	12 (23.5)	
Indeterminate	2 (14.3)	0 (0.0)	2 (3.9)	
Combined assessment				< 0.001
Viable	3 (21.4)	34 (91.9)	37 (72.5)	
Nonviable	9 (64.3)	3 (8.1)	12 (23.5)	
Indeterminate	2 (14.3)	0 (0.0)	2 (3.9)	

Visual Assessment	Nonviable Lesion (*n* = 14)	Viable Lesion (*n* = 37)	Total (*n* = 51)	*p*
Dual imaging helpful				< 0.001
Yes	7 (50.0)	34 (91.9)	41 (80.4)	
No	7 (50.0)	3 (8.1)	10 (19.6)	

Note—Values are the number (percentage) unless indicated otherwise. Early and delayed phase images were obtained at 30 minutes (time 1) and 3 hours (time 2), respectively.

TABLE 2:

Comparison of Semiquantitative Parameters for Both Viable and Nonviable Lesions

Parameter	Nonviable Lesion (*n* = 14)	Viable Lesion (*n* = 37)	Total (*n* = 51)	*p*
SUV_{max}				
Lesion				
Early phase	5.6 (0.7–8.9)	10.3 (4.6–16.4)	9.0 (0.7–16.4)	< 0.001
Delayed phase	7.4 (1.1–14.9)	16.0 (5.9–62.5)	13.6 (1.1–62.5)	0.003
p	0.010[a]	< 0.001[a]		0.180[b]
CWM				
Early phase	4.1 (2.3–6.21	4.3 (2.7–10.0)	4.0 (2.3–10.0)	0.662
Delayed phase	4.8 (2.8–7.41	4.5 (2.2–6.71	4.6 (2.2–7.41	0.468
p	0.049	0.358	0.420	
Contralateral caudate nucleus head				
Early phase	11.8 (6.4–14.8)	12.6 (7.1–25.4)	12.4 (6.4–25.4)	0.475
Delayed phase	15.7 (8.1–21.7)	15.2 (4.8–30.2)	14.4 (4.8–30.2)	0.793
p	< 0.001	< 0.001	0.533	
Ipsilateral CC				
Early phase	8.1 (5.2–10.8)	9.2 (6.0–14.6)	8.9 (5.2–14.6)	0.067
Delayed phase	9.6 (5.8–13.0)	9.7 (5.3–14.7)	9.6 (5.3–14.7)	0.952
p	0.009	0.081	0.255	
Lesion to CWM				
Early phase	1.4 (0.2–2.1)	2.5 (1.0–4.6)	2.2 (0.2–4.6)	< 0.001
Delayed phase	1.7 (0.2–3.5)	3.6 (1.3–9.9)	3.0 (0.2–9.9)	< 0.001
p	0.147[a]	< 0.001[a]		0.152[b]
Lesion to contralateral caudate nucleus head				
Early phase	0.5 (0.1–0.8)	0.9 (0.4–1.5)	0.8 (0.1–1.5)	< 0.001
Delayed phase	0.5 (0.1–0.8)	1.1 (0.4–3.5)	0.9 (0.1–3.5)	< 0.001
p	0.984[a]	< 0.001[a]		0.176[b]
Lesion to ipsilateral CC				
Early phase	0.7 (0.1–1.0)	1.1 (0.6–1.9)	1.0 (0.1–1.9)	< 0.001
Delayed phase	0.8 (0.1–1.6)	1.7 (0.6–6.0)	1.4 (0.1–6.0)	0.001

AJR Am J Roentgenol. Author manuscript; available in PMC 2021 October 01.

Parameter	Nonviable Lesion (*n* = 14)	Viable Lesion (*n* = 37)	Total (*n* = 51)	*p*
p	0.227[a]	< 0.001[a]		0.124[b]
Ratio of ratios	1.1 (0.9–2.2)	1.5 (0.7–4.3)	1.4 (0.7–4.3)	0.118
Percent change				
Lesion SUV_{max}	31.4 (−26.0 to 69.1)	55.8 (−4.9to458.0)	49.1 (−26.0 to 458.0)	0.317
Lesion to CWM	14.1 (−13.5 to 120.8)	48.4 (−27.0 to 334.0)	39.0 (−27.0 to 334.0)	0.118
Lesion to contralateral caudate nucleus head	0.5 (−41.5 to 33.0)	26.3 (−30.4 to 157.3)	19.2 (−41.5 to 157.3)	0.018
Lesion to ipsilateral CC	14.41 (−33.7 to 86.3)	47.5 (−16.1 to 346.4)	38.4 (−33.7 to 346.4)	0.092

Note—Values are the mean (range) unless indicated otherwise. Early and delayed phase images were obtained at 30 (time 1) and 90 (time 2) seconds, respectively. SUV_{max} = maximum standardized uptake value, CWM = contralateral white matter, CC = cerebellar cortex.

[a]From paired *t* test.

[b]From assessment of interaction between nature of lesion and phase.

TABLE 3:

Optimal Cutoff Values Based on ROC Analysis and Associated Measures of Diagnostic Performance

Parameter	AUC (%)	Optimal Cutoff[a]	Accuracy		p^b	Sensitivity	Specificity	PPV	NPV
			Value	95% CI					
SUV_{max}									
Lesion									
Early phase	92.1	7.20	45/51 (88.2)	76–96	0.006	33/37 (89.2)	12/14 (85.7)	33/35 (94.3)	12/16 (75.0)
Delayed phase	87.5	7.80	46/51 (90.2)	79–97	0.001	36/37 (97.3)	10/14 (71.4)	36/40 (90.0)	10/11 (90.9)
Lesion to CWM									
Early phase	89.0	2.05	42/51 (82.4)	69–91	0.070	29/37 (78.4)	13/14 (92.9)	29/30 (96.7)	13/21 (61.9)
Delayed phase	88.7	2.36	42/51 (82.4)	69–91	0.070	30/37 (81.1)	12/14 (85.7)	30/32 (93.8)	12/19 (63.2)
Lesion to CCH									
Early phase	88.6	0.68	42/51 (82.4)	69–91	0.070	29/37 (78.4)	13/14 (92.9)	29/30 (96.7)	13/21 (61.9)
Delayed phase	90.8	0.61	43/51 (84.3)	71–93	0.030	32/37 (86.5)	11/14 (78.6)	32/35 (91.4)	11/16 (68.8)
Lesion to ipsilateral CC									
Early phase	87.3	0.89	42/51 (82.4)	69–91	0.070	30/37 (81.1)	12/14 (85.7)	30/32 (93.8)	12/19 (63.2)
Delayed phase	87.4	1.07	41/51 (80.4)	67–90	0.130	31/37 (83.8)	10/14 (71.4)	31/35 (88.6)	10/16 (62.5)
Percent change									
Lesion to CCH	73.7	14.20[c]	36/51 (70.6)	56–83	0.680	35/37 (94.6)	11/14 (78.6)	25/28 (89.3)	11/23 (47.8)

Note—Values are the number/total number (percentage) unless indicated otherwise. Early and delayed phase images were obtained at 30 minutes (time 1) and 3 hours (time 2), respectively. PPV = positive predictive value, NPV = negative predictive value, SUV_{max} = maximum standardized uptake value, CWM = contralateral white matter, CCH = contralateral caudate nucleus head, CC = cerebellar cortex.

[a] Optimal cutoff values were determined after ROC analysis.

[b] Values indicate whether the accuracy is greater than the no-information rate, which is the percentage of the largest class (viable or nonviable tumor) for each parameter.

[c] Only lesion–to–contralateral caudate nucleus head percent change showed a statistically significant result with a markedly lower AUC value.

TABLE 4:

Subgroup Comparison of Cases With Available Perfusion MR Images Using Predictions Based on Specific Cutoff Values

Measured Value, Predicted Outcome[a]	True Outcome: Nonviable Lesion (*n* = 8)	True Outcome: Viable Lesion (*n* = 12)	Total (*n* = 20)	Accuracy	*p*[b]	Sensitivity (%)	Specificity (%)
Perfusion DSC-MRI							
rCBV				60 (36–81)	0.60	83.0	25.0
Nonviable	2	2	4				
Viable	6	10	16				
rPH				60 (36–81)	0.60	83.0	25.0
Nonviable	2	2	4				
Viable	6	10	16				
PET/CT							
Lesion SUV_{max}				80 (56–94)	0.05	75.0	87.5
Early phase							
Nonviable	7	3	10				
Viable	1	9	10				
Delayed phase				85 (62–97)	0.01	91.7	75.0
Nonviable	6	1	7				
Viable	2	11	13				
Lesion to CWM SUV_{max}				75 (50–90)	0.12	58.3	100.0
Early phase							
Nonviable	8	5	13				
Viable	0	7	7				
Delayed phase				80 (56–94)	0.05	66.7	100.0
Nonviable	8	4	12				
Viable	0	8	8				

Note—Values in parentheses are 95% CIs. Early and delayed phase images were obtained at 30 minutes (time 1) and 3 hours (time 2), respectively. DSC = dynamic susceptibility contrast, rCBV = relative cerebral blood volume, rPH = relative peak height, SUV_{max} = maximum standardized uptake value, CWM = contralateral white matter.

[a]Predictions were made using the following cutoff values: rCBV, 2.1; rPH, 1.38; lesion SUV_{max} on early phase imaging, 7.2; lesion SUV_{max} on delayed phase imaging, 7.8; lesion to CWM SUV_{max} on early phase imaging, 2.05; lesion to CWM SUV_{max} on delayed phase imaging, 2.36.

[b] Values indicate whether the accuracy is more than the no-information rate, which is the percentage of the largest class (viable or nonviable tumor) for each parameter.